Microwave Attenuation Measurements in Satellite-Ground Links: The Potential of Spectral Analysis for Water Vapor Profiles Retrieval

Fabrizio Cuccoli, Luca Facheris, Simone Tanelli, *Member, IEEE,* and Dino Giuli, *Senior Member, IEEE*

***Abstract*—In this paper, we address the problem of estimating vertical profiles of atmospheric water vapor by means of attenuation measurements simultaneously made at different frequencies along a vertical satellite-ground link. The operating frequencies selected are those around the spectral absorption lines of water vapor at 22.235 GHz. A simulation is presented of multifrequency attenuation measurements, based on an atmospheric propagation model and on radiosonde data providing true profiles of temperature, pressure, and water vapor. The results indicate that such multifrequency measurements are correlated to variations of the vertical profiles of water vapor. It is therefore expected that vertical detail of such profiles depends on number and position of the frequencies utilized.**

***Index Terms*—Attenuation measurements, radiosondes, spectral analysis, vertical profiles, water vapor.**

I. Introduction

In recent years, the analysis of vertical profiles of water vapor attracted growing interest due to the increasing use of Ka and Ku bands in communication satellites. In such bands, the attenuation due to water vapor may become relevant. For applications of interest in the communications area, combined attenuation and emission measurements were performed to design satellite links at 20/30 GHz. Obviously, the objective of the research in the communications area was to define the optimal frequencies for transmission in the cited frequency range. For this purpose, statistically consistent results were obtained for the whole range. In fact, a great number of measurements were carried out in different climatical, seasonal, and daily (diurnal and nocturnal) conditions [1].

From a different point of view, the aforementioned results induced us to investigate the possibility of exploiting multifrequency attenuation measurements made along transmitter-receiver links for remote sensing applications involving the estimation of the vertical profiles of water vapor. In this framework in fact, currently only multifrequency radiometers data permit to perform such estimates. However, the limitations of radiometer-based retrieval of water vapor profiles are well known (see for instance [2]–[4]), such as the relevant uncertainties about the emissivity function (temperature profile, source emissivity, etc.). In addition to that, spaceborne microwave radiometers suffer from a basic spatial resolution problem, related to their standard field of view. Also, the large bandwidth required to increase the received power of radiometers, and their sensitivity does not allow a sufficiently fine spectral resolution as would be required to determine the shape of the vertical profiles with the precision needed in applications requiring the in depth analysis of local atmospheric conditions.

The use of an active system based on a simple transmitter-receiver link at microwaves can indeed overcome some of the aforementioned drawbacks. Firstly, the possibility to increase the transmitted power while decreasing the receiver's bandwidth allows us to minimize the effects of noise in reception. Secondly, the point-to-point link geometry directly eliminates problems of horizontal spatial resolution.

In this paper, we present a detailed spectral analysis of the atmospheric attenuation effects generated by vertical profiles of water vapor around the 22.235 GHz absorption line. The objective of such analysis is to introduce a method, based on multifrequency differential attenuation measurements made by a transmitter-receiver pair along an Earth-satellite link and to investigate how water vapor profiles are correlated to the spectral attenuation characteristics of the link. The conclusion of such analysis is that, making attenuation measurements at multiple frequencies around 22.235 GHz, it is possible to exploit the variations of the absorption characteristics with height, which depend in turn on the height variations of temperature and pressure, to retrieve information about the vertical profile of water vapor.

Since narrowband and multifrequency vertical attenuation measurements in the range 18 (30 GHz are not available; the aforementioned spectral analysis has been performed through simulations of attenuation measurements based on a standard propagation model and standard atmospheric composition models (Section III). In such a manner, it is possible to evaluate and discuss (in Section IV) the variations of the spectral absorption characteristics with the atmospheric conditions. Based on such spectral analysis, a spectral sensitivity function is defined, directly depending on the profile's shape. The objective of the final part of the paper (Section V) is to test the spectral sensitivity function on real attenuation data. These are derived, (aside from the cited propagation model), from real vertical profiles of temperature, pressure, and water vapor gathered by radiosondes located in Bologna, Italy and Bordeaux, France, in different daily and seasonal conditions.

Manuscript received November 12, 1999; revised June 23, 2000. This paper was supported by the National Research Council (CNR/GNDCI) and by the Italian Ministry for Scientific/Technological Research.

The authors are with the Dipartimento di Elettronica e Telecomunicazioni, Università di Firenze, 50139 Firenze, Italy (e-mail: facheris@ingfi1.ing.unifi.it).

Publisher Item Identifier S 0196-2892(01)02085-X.

II. Basic Issues of Microwave Propagation Along Vertical Paths in the Atmosphere

The basic measurement scheme to which we refer in the following is that sketched in Fig. 1, where z_{tx} and z_{rx} are the transmitter and the receiver positions, respectively. The spectral radiance received can be expressed using the formal solution of the one-dimensional (1-D) radiative transfer equation [5]

$$J(z_{rx},f)=J(z_{tx},f)e^{-\tau(z_{tx},z_{rx},f)}+\int_{z_{tx}}^{z_{rx}}S(z,f)e^{-\tau(z,z_{rx},f)}\,dz \tag{1}$$

where

f frequency in Hz,
$J(z_{tx},f)$ spectral radiance in z_{tx},
$S(z,f)$ accounts for the emission contributions between z and $z+dz$ along the integration path;
$\tau(z_1,z_2,f)$ optical depth.

This is defined as follows:

$$\tau(z_1,z_2,f)=\int_{z_1}^{z_2}k(z,f)\,dz \tag{2}$$

where $k(z,f)$ is the extinction coefficient of the propagation medium accounting for power losses between z and $z+dz$.

Assuming that the transmitter is a point source and that the first term of (1) is much greater than the second one (i.e., that the emission contribution $S(z,f)$ is negligible compared to the transmitted spectral radiance), the Beer-Lambert law of exponential attenuation (in terms of spectral irradiance) holds [6]

$$I(z_{rx},f)=I(z_{tx},f)e^{-\tau(z_{tx},z_{rx},f)}. \tag{3}$$

Let us define the spectral attenuation $A(f)$ as the ratio between the transmitted and received spectral irradiances. Using (2) and (3) and expressing $A(f)$ in neper, we obtain

$$A(z_1,z_2,f)=\tau(z_1,z_2,f). \tag{4}$$

The extinction coefficient $k(z,f)$ is usually expressed as the sum of an absorption coefficient $k_a(z,f)$ and of a scattering coefficient $k_s(z,f)$. The former accounts for the energy losses due to molecular absorption, while the latter accounts for all other attenuation contributions such as those due to scattering from fog, dust, clouds etc.

The absorption coefficient $k_a(z,f)$ comes from the contribution of all molecular species contained in $[z,z+dz]$

$$k_a(z,f)=\sum_i k_{ai}(z,f) \tag{5}$$

where $k_{ai}(z,f)$ is the absorption coefficient of the ith molecular species.

The absorption properties of each molecular species are commonly accounted for through the absorption cross section σ_a of the species in question. (σ_a is defined as the quantity that, multiplied by the concentration of the species, gives the absorption coefficient k_a. Therefore, for the generic ith species

$$k_{ai}(z,f)=N_i(z)\sigma_{ai}(z,f) \tag{6}$$

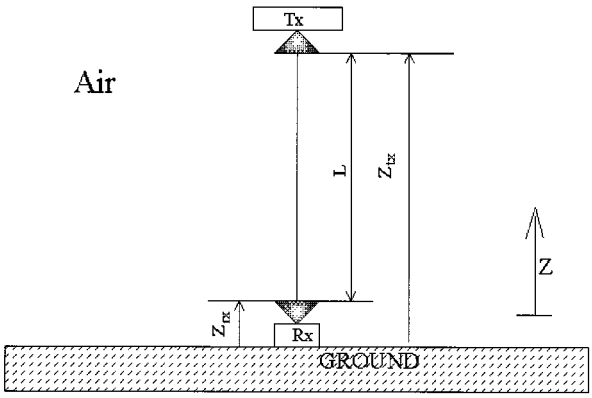

Fig. 1. Simple scheme of an atmospheric transmitter-receiver pair.

where $N_i(z)$ is the vertical concentration profile of the ith molecular species.

Expressing N_i in molecules per cm^3, σ_{ai} is in cm^2 per molecule. The value of σ_{ai} at a given frequency is determined by the contributions of all the absorption lines (due to the vibro-rotational transitions among molecular energetic levels) of the ith molecular species.

The absorption coefficients depend on the altitude z since the absorption characteristics directly depend on pressure $P(z)$, temperature $T(z)$ and concentrations of all species present in the infinitesimal interval $[z,z+dz]$.

If the partial pressure of the ith molecular species is negligible compared to the total pressure (barometric pressure), $\sigma_{ai}(z)$ is independent of the concentration and can be thus determined through $T(z)$ and $P(z)$ only. This holds for those molecular species (like CO, NO, O_3, NO_2), whose concentrations are much smaller than the sum of all molecular atmospheric components, but the absorption cross sections of the major atmospheric components (i.e., N_2, O_2, H_2O, and CO_2) depend also on their concentrations.

III. Computation of Attenuation Measurements Through an Atmospheric Propagation Model

As outlined in the introduction, our primary task was to evaluate the spectral attenuation properties of the atmosphere through a propagation model. For this purpose, we referred to the basic equations of the Millimeter-Wave Propagation Model (MPM) for moist air developed by Liebe [7]. The MPM permits to compute the extinction coefficients for meteorological variables up to 130 km altitude and for frequencies smaller than 1000 GHz. It is mainly based on O_2 and H_2O spectroscopic parameters related to absorption spectral lines up to 1000 GHz. Five absorption contributions have been accounted for:

$k_{(O_2)_R}$ O_2 absorption, based on 44 spectral lines up to 834 GHz;
$k_{(w)_R}$ water vapor absorption, based on 34 spectral lines up to 988 GHz;
$k_{(O_2)_C}$ O_2 nonresonant absorption terms;
$k_{(N_2)_C}$ N_2 nonresonant absorption terms;
$k_{(w)_C}$ H_2O continuum spectrum.

Let us define $k_w(z,f)$ and $k_{OTHERS}(z,f)$ as the absorption coefficients accounting, respectively, for the single contribution

of water vapor and for the total contribution of all other species. Equation (2) can then be rewritten as

$$\tau(z_1, z_2, f) = \int_{z_1}^{z_2} (k_w(z, f) + k_{OTHERS}(z, f))\, dz. \quad (7)$$

Accordingly

$$k_w(z, f) = k_{(w)_R}(z, f) + k_{(w)_C}(z, f) \quad (8)$$

$$k_{OTHERS}(z, f) = k_{(O_2)_R}(z, f) + k_{(O_2)_C}(z, f) + k_{(N_2)_C}(z, f). \quad (9)$$

Attenuation effects due to the scattering phenomenon were not considered. This is justified when assuming, as done in this work, that humidity is lower than 100% at every altitude.

As mentioned in Section II, the absorption coefficients depend on temperature, pressure, and on molecular concentration values. In the frequency interval of interest, concentration values of water vapor, O_2, and N_2 are sufficient to determine the total absorption coefficient. O_2 and N_2 make up the 99% of the dry air contents and are uniformly mixed up to several km altitude. Therefore, the pressure of dry air is sufficient to determine the N_2 and O_2 concentration. The same does not hold for water vapor.

The concentration of water vapor is generally given in terms of n.molec/cm^3 and/or relative humidity. Under the assumption of ideal gas conditions, these two quantities are related as follows:

$$N_w = 7.2435 \cdot 10^{16} \cdot \frac{1}{T} \cdot P_s \cdot RH_{\%} \quad (10)$$

where N_w and $RH_{\%}$ are the water vapor contents expressed respectively as n.molec/cm^3 and percentage relative humidity (between 0 and 100), P_s is the saturation pressure of H_2O in mbar, and T is the temperature in Kelvin. P_s depends on temperature only. Approximately, it is given by [7]

$$P_s = 2.408 \cdot 10^{11 \cdot \theta^5} \cdot e^{-22.644 \cdot \theta^5} \quad (11)$$

where $\theta = 300/T$.

Therefore, the input variables needed to compute (8) and (9) at frequency f and used in the following for this purpose are barometric pressure, temperature, and water vapor concentration at altitude z.

By applying the propagation model jointly with the standard summer atmosphere (SSA) referring to the European latitudes [8], we get immediate evidence of the variations of spectral attenuation contributions with height. In particular, in the frequency interval around 22 GHz, $k_{(w)_R}$ gives the main attenuation contribution at lower altitudes (approximately below 10 km). At higher altitudes (approximately above 10 km), the attenuation contribution due to O_2 is such that the 22.235 GHz absorption line of the water vapor is not as dominant as at lower altitudes. These behaviors are well pointed out by Figs. 2 and 3. They show, respectively, at ground and at 15 km altitude, the five attenuation contributions (separate from each other) that we accounted for below 200 GHz. Both figures were obtained using the aforementioned SSA, whose vertical profiles of temperature, pressure, and water vapor concentration up to 15 km are plotted in Fig. 4.

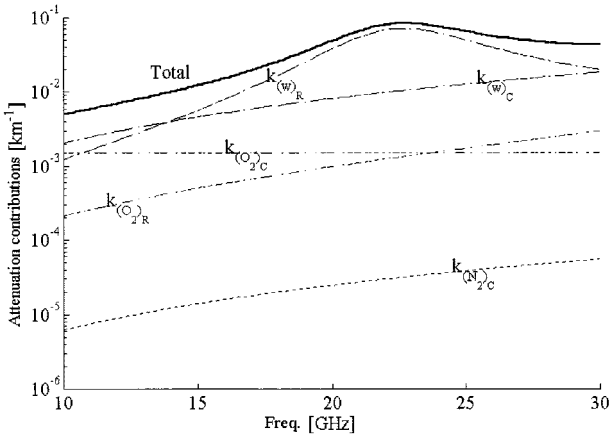

Fig. 2. Attenuation contributions at ground. $T = 294°$K, $P = 1013$ mb, and $RH_{\%} = 80\%$.

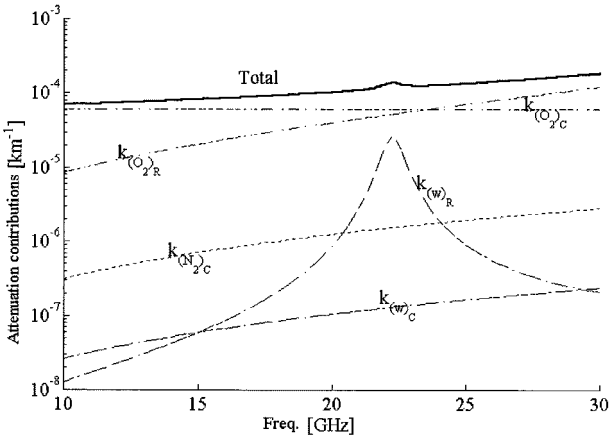

Fig. 3. Attenuation contributions at 15 km altitude. $T = 216°$K, $P = 130$ mb, and $RH_{\%} = 3\%$.

IV. Sensitivity of the Spectral Attenuation

In this section, we focus on the sensitivity of the spectral attenuation characteristics with respect to the shape variations of the vertical profiles of temperature, pressure, and water vapor. Such an analysis aims at providing a quantitative definition of the influence of each of the three profiles in order to individuate the most adequate frequencies for our measurement objectives.

As shown in the preceding section, the atmospheric layers giving significant contributions to the spectral attenuation in the frequency range considered are those up to 10–15 km altitude. This is true independent of the shape of the vertical profiles of temperature, pressure, and water vapor. The reason is that air density decreases with height according to an approximately exponential decay. Since water vapor is always present, a few kilometers are sufficient to obtain the total attenuation. Spectral attenuation has been computed by numerically approximating (7), and the results for the SSA model are shown in Fig. 5, which reports $A(z_1, z, f)$ considering $z_1 = 0$. The percentage increment of the total attenuation related to each atmospheric layer is shown as well. Notice that above 15 km the attenuation contributions is less than 0.1% of the total attenuation, and therefore can be neglected.

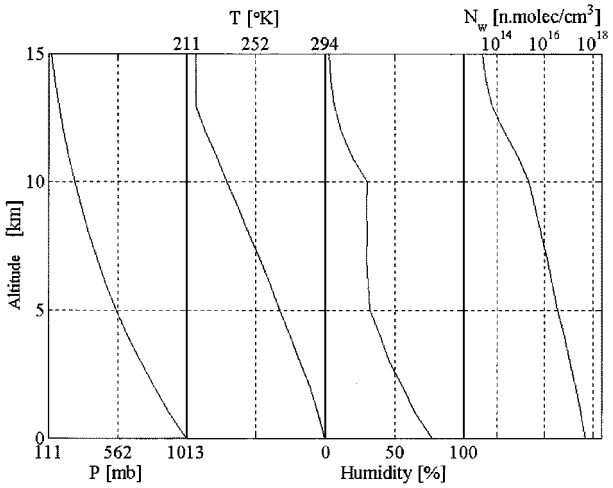

Fig. 4. Vertical profiles of temperature, pressure, and water vapor as from SSA up to 15 km altitude.

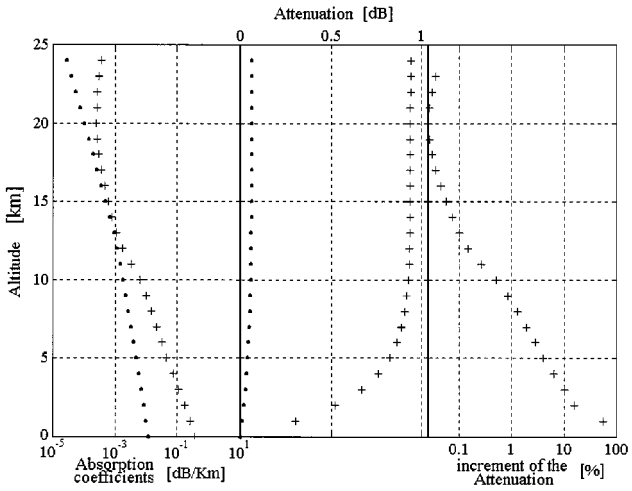

Fig. 5. Spectral attenuation function $A(z_1, z, f)$ up to 25 km altitude for $f = 22.235$ GHz and $z_1 = 0$ using the SSA model ($+k_w$, $\cdot$ (k_{OTHERS}). Left: absorption coefficients. Center: spectral attenuation. Right: percentage increment (step 1 km) of the spectral attenuation related to the first 15 Km of the atmosphere.

In the following, integration from $z_1 = 0$ to $z_2 = 15$ km is denoted by the superscript 0. Accordingly, we write the spectral attenuation as

$$A^{(0)}(f) = A(z_1, z_2, f)\big|_{\substack{z_1=0 \\ z_2=15}}. \tag{12}$$

To verify the influence of the vertical profiles of water vapor, temperature and pressure, let us first define two simple spectral sensitivity functions. The first, $R(f)$, is the incremental ratio of the spectral attenuation function

$$R(f) = \frac{A(f) - A(f - \Delta f)}{\Delta f} \tag{13}$$

while the second, $S(f)$, is the normalized incremental ratio of the spectral attenuation

$$S(f) = \frac{R(f)}{A(f)}. \tag{14}$$

Fig. 6 shows $A^{(0)}(f), R^{(0)}(f)$ and $S^{(0)}(f)$ referred to the SSA model, taken in the following as reference model for profiles and indicated by the subscript *ref*. In order to evaluate quantitatively the sensitivity of $A(f), R(f)$ and $S(f)$ to the variations of vertical profiles, we referred to the three following differential spectral functions, accounting, respectively, for the following:

1) the absolute deviation of $A(f)$ from the reference SSA case

$$\Delta A(f) = A(f) - A_{ref}(f) \tag{15}$$

2) the relative deviation of $R(f)$ from the reference SSA case

$$\Delta R(f) = \frac{R(f) - R_{ref}(f)}{R_{ref}(f)} \tag{16}$$

3) the relative deviation of $S(f)$ from the reference SSA case

$$\Delta S(f) = \frac{S(f) - S_{ref}(f)}{S_{ref}(f)}. \tag{17}$$

The sensitivity to the temperature and pressure profiles has been evaluated by randomly generating 100 temperature profiles and 100 pressure profiles. At a generic height, the respective values have been generated as independent random variables, uniformly distributed between $x_0(z)(1-p)$ and $x_0(z)(1+p)$, where $x_0(z)$ is the value of the reference profile (whether $T_0(z)$ or $P_0(z)$). We chose $p = 0.02$ and $p = 0.05$ for pressure and temperature profiles, respectively.

Figs. 7 and 8 show the variation ranges of the three differential spectral functions pertinent to temperature and pressure variations, respectively. The most important result of this investigation is that the uncertainty of the pressure profiles (less than 2%) and temperature profiles (less than 5%) causes an uncertainty on the attenuation less than 0.01 dB. Moreover, pressure variations do not influence $A^{(0)}(f)$ around 20.6 GHz, and neither does $R^{(0)}(f)$ or $S^{(0)}(f)$ around 18.8 GHz, while temperature variations have no practical influence on $R^{(0)}(f)$ around 20 GHz and on $S^{(0)}(f)$ around 19.8 GHz.

Different conclusions can be drawn for the vertical profiles of water vapor. We considered ten different vertical profiles modified starting from the SSA. As shown in Fig. 9(a), each profile reaches 100% humidity at a different altitude (from 1 to 10 km, step 1 km) and the water vapor amount added around that altitude is removed at ground so as to keep the same integrated water vapor content (IWV) of the SSA. Such a constraint is imposed so as to better point out the correlation between $\Delta R^{(0)}$ or $\Delta S^{(0)}$ and the effects of remarkable humidity gradients in the atmospheric layers. Fig. 9(b)–(d) shows, respectively, $\Delta A^{(0)}, \Delta R^{(0)}$ and $\Delta S^{(0)}$, considering such water vapor profiles.

The shape variations of vertical profiles cause small attenuation differences (less than 0.03 dB). However, note that the shape of $\Delta S^{(0)}$ depends remarkably on that of the vertical profiles of water vapor. In particular, the variation at low and at high frequencies depends on the variation at low and high altitudes, respectively.

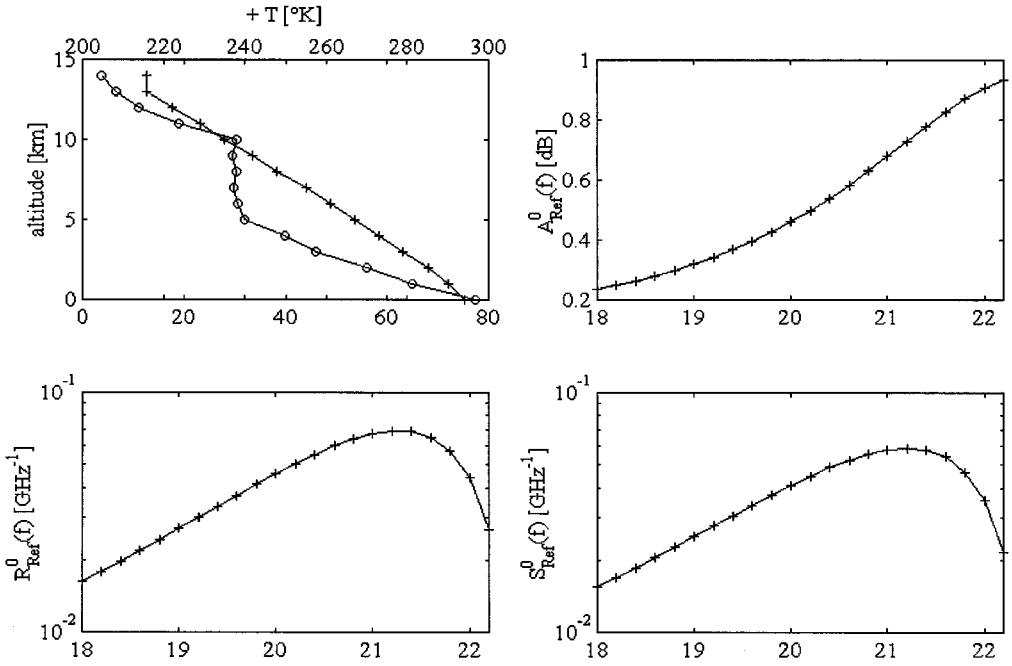

Fig. 6. Spectral sensitivity functions. (a) SSA vertical profiles of temperature (+) and water vapor (∘), (b) $A^{(0)}(f)$, (c) $R^{(0)}(f)$, and (d) $S^{(0)}(f)$.

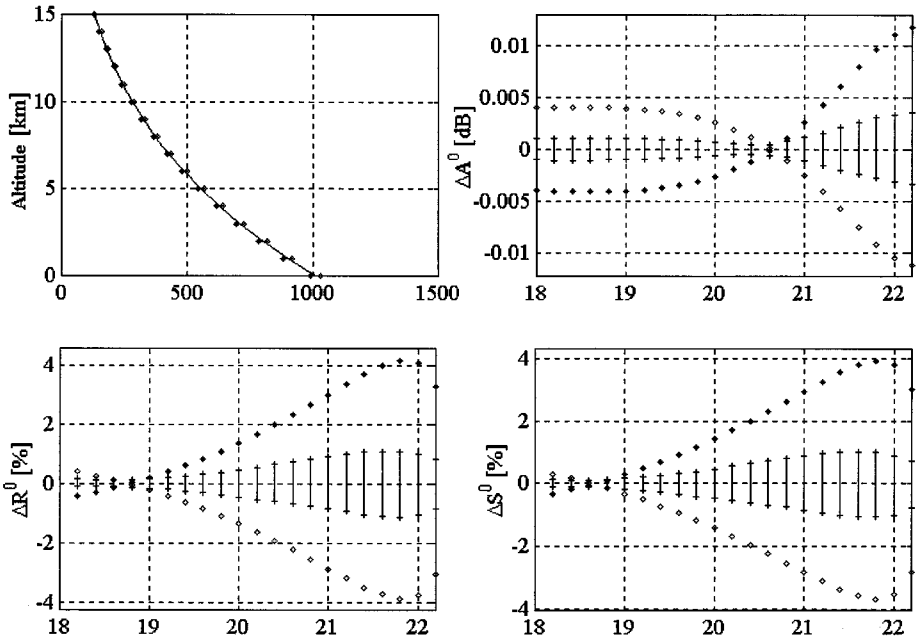

Fig. 7. Variation bars of the differential functions related to the SSA model. 100 pressure profiles are considered. (a) Pressure profile and variation bars, (b) $\Delta A^{(0)}$, (c) $\Delta R^{(0)}$, and (d) $\Delta S^{(0)}$. Star and diamond markers refer to the lowest and the highest pressure profile considered, respectively.

Notice that when humidity gradients occur at the lowest atmospheric layers (about 0–2 km), then $\Delta R^{(0)}$ and $\Delta S^{(0)}$ take values comparable to those shown in Figs. 7(c)–(d) and 8(c)–(d). Therefore, in this case, it is impossible to relate the sensitivity functions $\Delta R^{(0)}$ and $\Delta S^{(0)}$ to the profile's shape (unless temperature and pressure profile are *a priori* known). It is opportune to recall that this holds assuming the same IWV. However, in general, the IWV is not known, and vertical humidity gradients may differ remarkably from those considered in Fig. 9(a).

Fig. 9(b) shows that the frequencies around 20 GHz are the least sensitive to the variations of profiles with the same IWV. Therefore, attenuation measurements around such frequencies carry information about the IWV, and can thus be directly exploited as rough estimates of the IWV itself. The question is whether, after having estimated the IWV in such manner, the sensitivity function is still correlated to the profile's shape and possibly carries information about the "goodness" of that estimate. This fundamental issue is the matter of the next section, where real radiosonde data are used to simulate spectral attenuation measurements, and estimates of IWV are made by scaling in amplitude a reference water vapor profile while minimizing a given error functional. After that, the sensitivity function $\Delta S(f)$

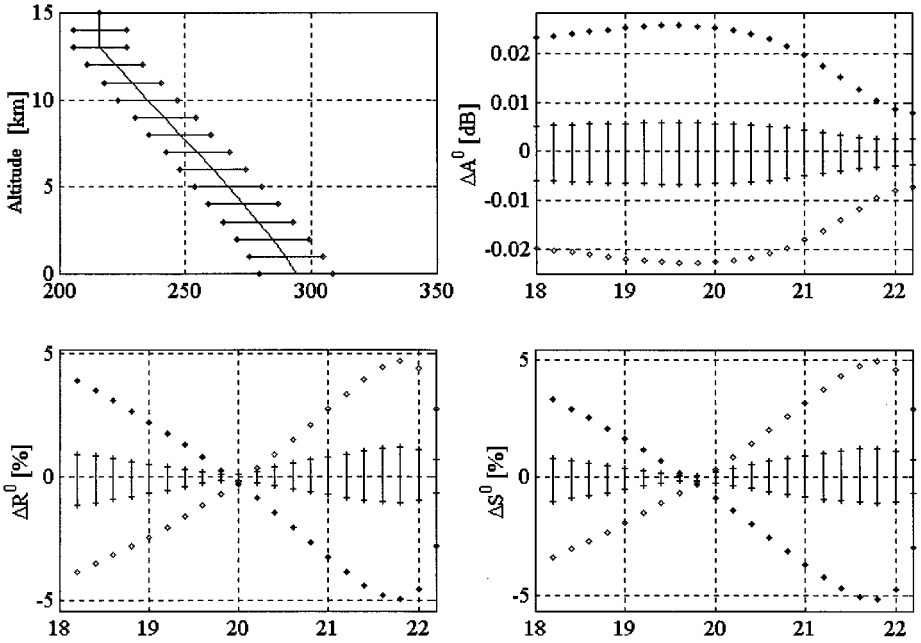

Fig. 8. Variation bars of the differential functions related to the SSA model considering 100 temperature profiles. Frame arrangement as in Fig. 7.

is evaluated and compared to the error between the real and the scaled profile.

V. Estimation of the IWV and Profile Error Analysis Based on Radiosonde Data

In order to overcome the unavailability of multifrequency attenuation measurements, the measurements of $A(f)$ and $S(f)$ were simulated for a set of frequencies of interest following the same approach discussed in Section III, but exploiting radiosonde data instead of the SSA model.

In the following, the simulated measurements will be referred to as "true measurements."

The algorithm developed starts from the attenuation measurements to estimate the IWV, assuming a given shape for the profile and scaling it through an iterative minimization procedure. Defining the initial vertical profile of water vapor as $N_0(z)$, the objective is to determine the scaling coefficient K that, multiplied by $N_0(z)$, minimizes the following error functional:

$$E(K) = \frac{1}{p} \sum_{i=1}^{N_f-1} \cdot \left(p_i \frac{(\widehat{A}_{i+1}(K) - \widehat{A}_i(K)) - (A_{i+1} - A_i)}{(A_{i+1} - A_i)} \right)^2 \quad (18)$$

where

- N_f number of frequencies utilized;
- p_i weighting coefficients, with $p = \Sigma_{1=1}^{N_f-1}\, p_i$;
- A_i attenuation value (in dB) at the ith frequency f_i (obtained from a radiosonde data set);
- $\widehat{A}_i(K)$ attenuation values (in dB) computed for the scaled profile $KN_0(z)$ at the ith frequency f_i.

The functional error is based on the differential attenuations $A_{i+1} - A_i$ in order to emphasize the water vapor contribution with respect to other attenuation contributions (for instance that due to molecular oxygen). In fact, since such contributions vary slowly with frequency (within the 18–22 GHz range) and the power measurements are made at close frequencies, they tend to cancel each other in $E(K)$. Moreover, assuming that the transmitted power level is independent of the emission frequency, the difference of two power measurements (in dB) would be independent of the transmitter power. If this assumption is not valid, the final attenuation estimated is obviously biased.

The weighting coefficients p_i are chosen such that the differential attenuation around 20 GHz gives the maximum contribution to $E(K)$. The reason for this choice is that, as mentioned in the previous section, the lowest sensitivity to the variations of the profile shape is around 20 GHz.

Once K is determined, the estimated integrated water vapor $\overline{IWV}$ is computed as

$$\overline{IWV} = \int KN_0(z)\, dz. \quad (19)$$

The relative error re_{IWV} of the IWV estimate is thus defined as follows:

$$re_{IWV} = \frac{\overline{IWV} - IWV}{IWV}. \quad (20)$$

To characterize the error on the profile obtained after the minimization procedure at each altitude, we used the following logarithmic function, which allows a correct representation of the greatest absolute errors:

$$pe(z) = \log_{10}\left[\frac{N_w(z)}{KN_o(z)}\right] \quad (21)$$

where $N_w(z)$ is the water vapor profile derived from the radiosonde data.

This simple minimization procedure was applied for different shapes of $N_0(z)$ and for different radiosonde data sets. Seven

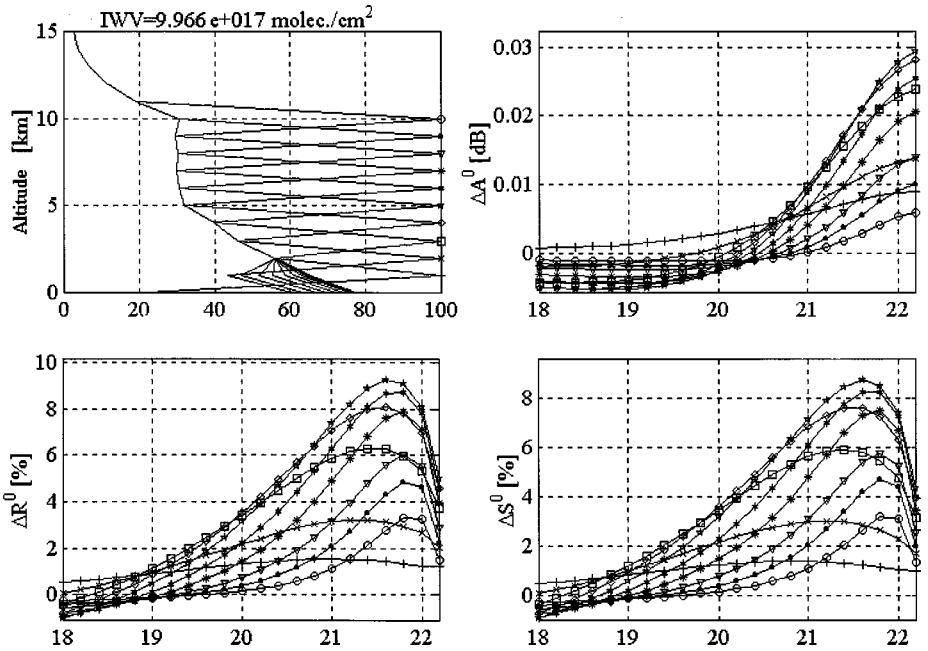

Fig. 9. Differential functions considering ten vertical profiles of water vapor having the same IWV of the SSA. (a) Vertical profiles of water vapor, (b) $\Delta A^{(0)}$, (c) $\Delta R^{(0)}$, and (d) $\Delta S^{(0)}$. Each marker refers to a different water vapor profile.

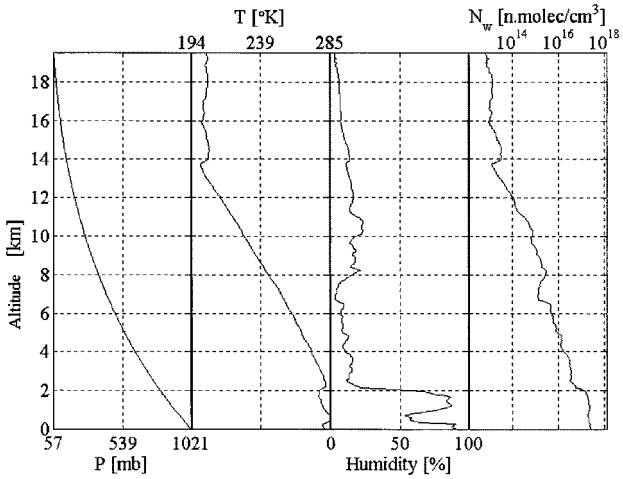

Fig. 10. Vertical profiles obtained by radio-sounding made on November 15, 1994 at 12:00 am nearby Bologna, Italy, up to 15 km altitude.

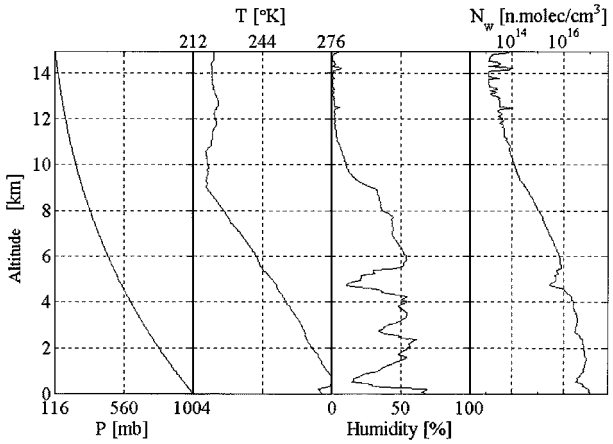

Fig. 11. Vertical profiles obtained by radio-sounding made on January 2, 1997 at 11:15 am in Bordeaux, France, up to 15 km altitude.

frequencies were used (from 19 to 22 GHz step 0.5 GHz) to simulate the measurements of $A(f)$ and $S(f)$. At the end of each minimization, re_{IWV} and the test function $\Delta S(f)$ were computed (as the ratio between the true $S(f)$ measurements and the retrieved $S(f)$ computed using $KN_0(z)$ as water vapor's vertical profile). Starting the minimization procedure with different physically plausible shapes of $N_0(z)$, we recorded values of re_{IWV} up to 15%. Therefore, independently of the profile used to start the minimization, the differential attenuation measurements allowed us to reach an acceptable estimate of IWV, that can be used as starting point for the following analysis of correlation between the profile error and the spectral sensitivity.

We report in the following three minimization cases among all those considered, that are typical and also representative of the correlation existing between the error profile and $\Delta S(f)$. The first two cases refer to a radio-sounding made on November 15, 1994 at 12:00 am in the neighborhoods of Bologna, Italy, reported in Fig. 10. The third one refers to a radio sounding made on January 2, 1997, at 11:15 am in Bordeaux, France, reported in Fig. 11.

In the first case considered, the SSA profile was used as $N_0(z)$. Fig. 12(a) and (b) shows the final vertical profile and pe(z), while Fig. 12(c) shows the test function $\Delta S(f_i)$, $i = 1, \cdots, 7$. In the second and third cases, reported in Figs. 13 and 14, respectively, $N_0(z)$ was chosen quite different from the SSA in order to verify whether the correlation between $pe(z)$ and the test function is maintained.

Notice first of all that while re_{IWV} takes acceptable values in all cases, the error profile $pe(z)$ changes substantially. Furthermore, comparing $pe(z)$ and $\Delta S(f_i)$ in the three cases, it

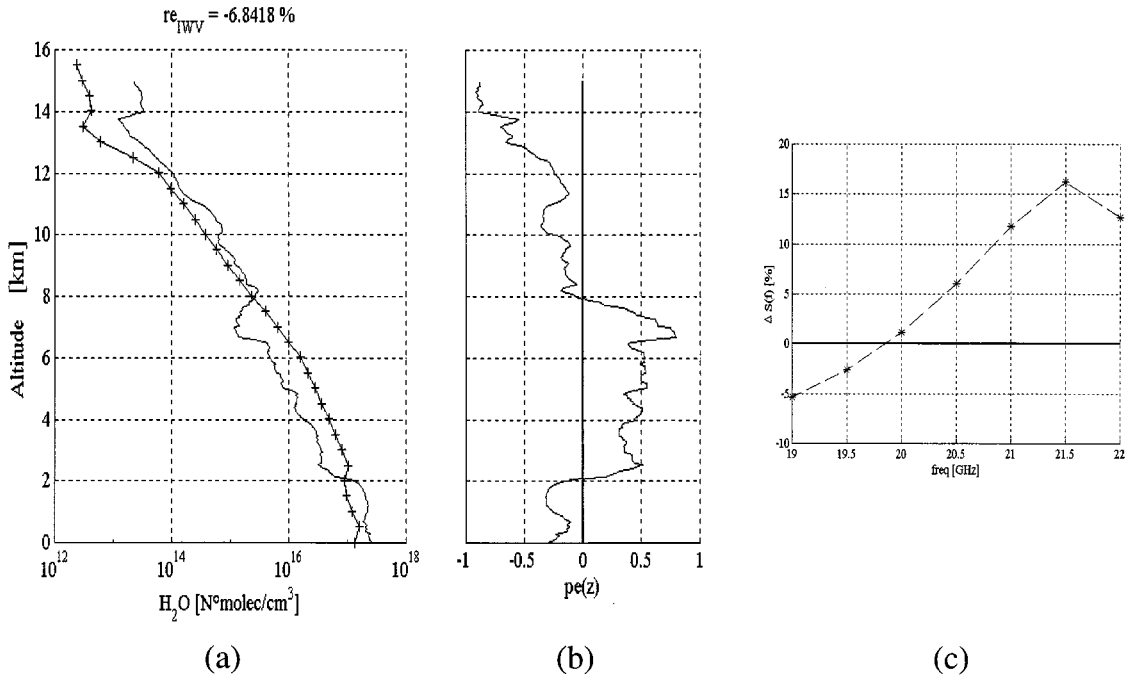

Fig. 12. First retrieval example (Bologna): (a) water vapor's vertical profiles. Continuous line: radiosonde profile. Cross line: retrieved profile. (b) Profile error and (c) $\Delta S(f)$ computed from 19 to 22 GHz step 0.5 GHz (seven frequencies).

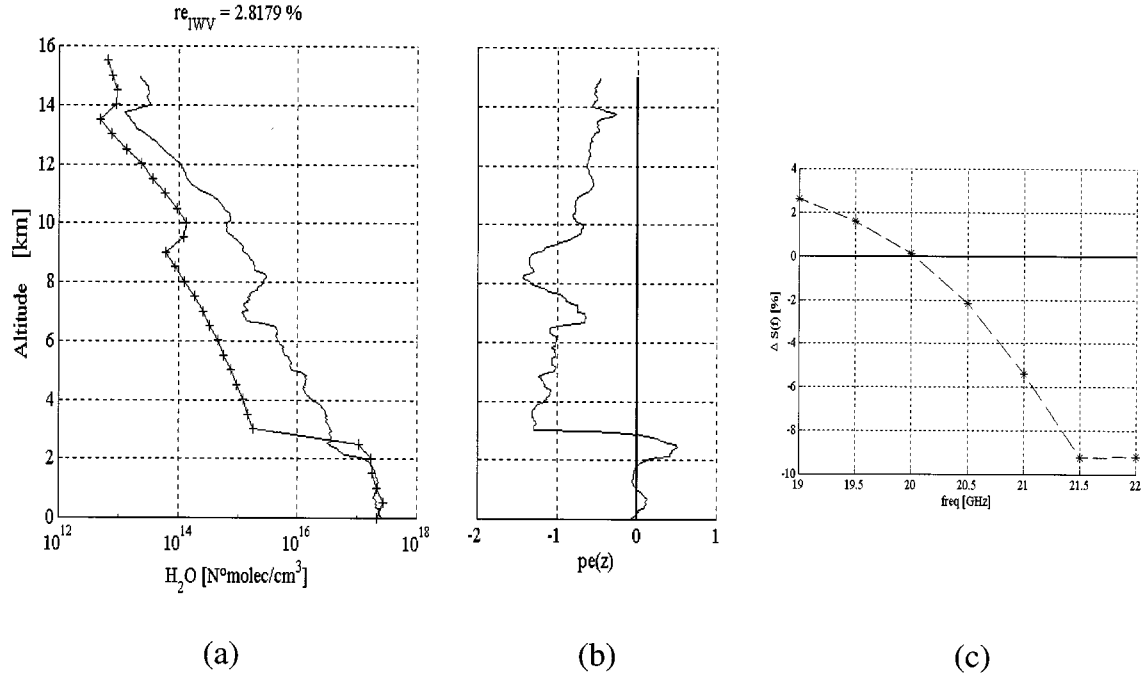

Fig. 13. Second retrieval example (Bologna, seven frequencies used). Figure arrangement as in Fig. 12.

is possible to notice their correlation. First notice that the two test functions of Figs. 12 and 14 exhibit an opposite behavior with respect to frequency, and this is correlated with the opposite signs of the two error profiles. In particular, the sign of $pe(z)$ at lower altitude (below about 2–3 km), at intermediate altitude (between 2–3 and 7–10 km), and at higher altitude (over 7–10 km) are correlated to the sign of $\Delta S(f_i)$, respectively, at lower (up to 20 GHz), intermediate (20 $\div$ 21 GHz), and higher frequencies (over 21–22 GHz). Furthermore, the amplitude of $\Delta S(f_i)$ is roughly correlated to the error amplitude. Finally, the upper frequency band 21 $\div$ 22 GHz is highly sensitive to errors over 8 $\div$ 10 km altitude. Note the fact that while $\Delta S(f_i)$ is characterized by a sharp maximum and minimum in the cases of Figs. 12 and 14 due to the sign reversal of the profile error at such altitudes, it settles around the minimum in Fig. 13 since in that case, the error keeps the same sign.

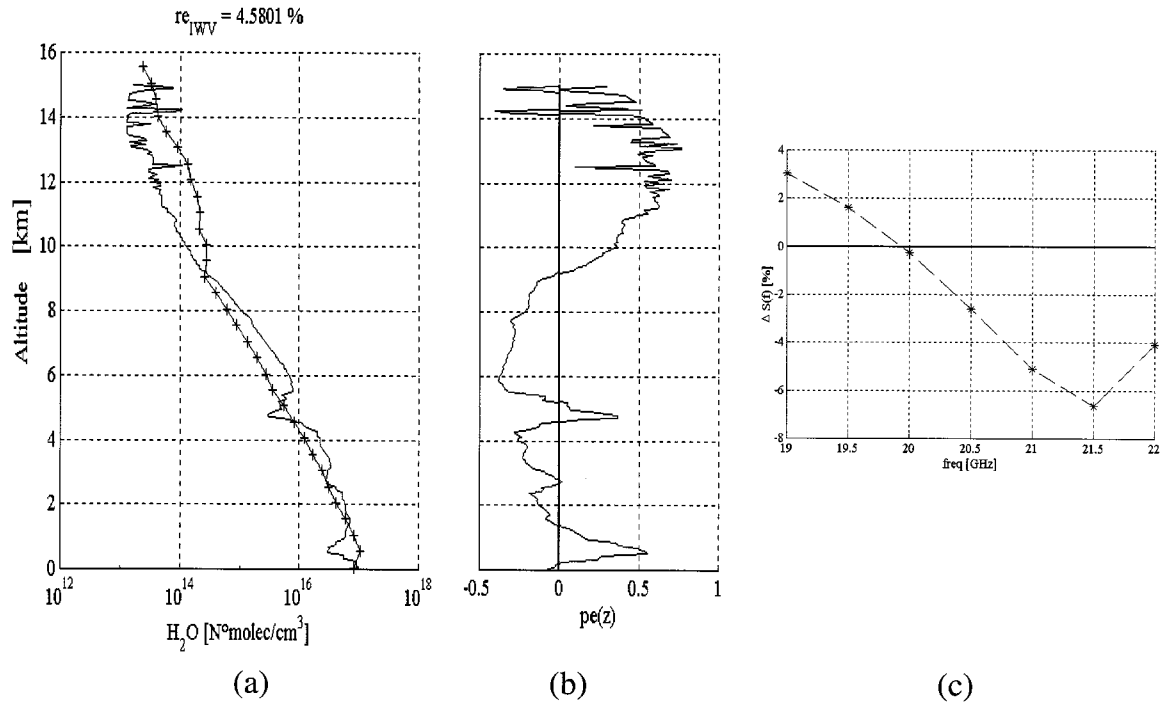

Fig. 14. Third retrieval example (Bordeaux, seven frequencies used). Figure arrangement as in Fig. 12.

VI. Conclusions

Thanks to the variations with altitude of the absorption characteristics of the atmosphere, multifrequency attenuation measurements made around 22.235 GHz along vertical paths can be exploited in a differential approach in order to define a spectral sensitivity function carrying information about the vertical profiles of water vapor. The greater variations with frequency of the absorption characteristics of water vapor with respect to the other atmospheric components make the differential approach adequate for evidencing the attenuation contribution by water vapor. Finally, a low sensitivity to the uncertainty on temperature and pressure profiles is expected based on the results presented.

The correlation elements evidenced in the last section between the error profiles and the test sensitivity function are common to the totality of cases analyzed. Therefore, the spectral analysis outlined exhibits an interesting potential that can be usefully exploited in iterative procedures for improving the profile estimate, in terms of both IWV and shape.

A peculiar characteristic of attenuation measurements based on a point-to-point link is that the water vapor profile is retrieved on a local scale. Such an approach could be complementary to radiometers since it can be exploited to analyze finer temporal and geographical modifications. Moreover, the use of an active system permits to overcome several intrinsic limitations of passive systems based on ground or spaceborne radiometers, such as the spatial resolution and the SNR at the receiver.

Currently, our objective is to implement the iterative algorithm to retrieve water vapor vertical profiles based only on attenuation measurements and on the related spectral sensitivity function, without requiring historical data sets and/or statistical hypotheses on location, climate, and atmospheric conditions. This is being carried out together with a feasibility study concerning primarily the optimal choice of 1) the number and position of significant frequencies; 2) the transmission system and related modulation; and 3) the influence of the receiver noise on spectral measurement accuracy.

Finally, since the sensitivity function requires a propagation model as reference to simulate attenuation measurements to be compared with variations of spectral attenuation properties with altitude, a model accuracy issue may indeed be posed. However, we envisage that, once a specific model is chosen, possible inaccuracies of its parameters (we refer in particular to inaccurate modeling of the dependence of such parameters on pressure and temperature) should have no significant influence on the sensitivity function (also thanks to the differential frequency approach). It is therefore expected that future improvements of the kind here, which adopted Liebe's model in terms of parameters' accuracy, shall not influence mentioned future iterative procedures for profile retrieval.

Acknowledgment

The authors wish to thank Dr. Captain G. Lenzi for having provided the Bologna radiosonde data, and Mr. L. Capannesi for his technical support.

References

[1] J. P. V. Poiares Baptista and P. G. Davie, "Reference book attenuation measurement and prediction," in *2nd Workshop OPEX*, 1994.

[2] Y. Han and E. R. Westwater, "Remote sensing of tropospheric water vapor and cloud liquid water by integrated ground-based sensors," *J. Atmos. Ocean. Technol.*, vol. 12, pp. 1050–1059.

[3] B. B. Stankov, E. R. Westwater, and E. E. Gossard, "Use of wind profiler estimates of significant moisture gradients to improve profile retrieval," *J. Atmos. Ocean. Technol.*, vol. 13, pp. 1285–1290.

[4] T. T. Wilheit, "An algorithm for retrieving water vapor proiles in clear and cloudy atmosphere from 184 GHz radiometric measurements: Simulation studies," *J. Appl. Meteorol.*, vol. 29, pp. 508–514.
[5] F. T. Ulaby, R. K. Moore, and A. K. Fung, *Microwave Remote Sensing*. Norwood, MA: Artech House, 1986, vol. I.
[6] R. M. Measures, *Laser Remote Sensing*. New York: Wiley, 1983.
[7] H. J. Liebe, G. A. Hufford, and M. G. Cotton, "Propagation modeling of moist air and suspended water/ice particles at frequencies below 100 GHz," in *AGARD Meeting on Atmospheric Propagation Effects through Natural and Man-Made Obscurants for Visible to MM-Wave Radiation*, Palma de Mallorca, Spain, May 1993.
[8] R. A. McClatchey, R. W. Fenn, J. E. Selby, A. Volz, and J. S. Garing, Optical properties of the atmosphere, in Rep. AFCRL-72-0497, Environ. Res. Papers, Air Force Cambridge Res. Lab., vol. 411.

Fabrizio Cuccoli received the laurea degree (cum laude) in electronic engineering and the Ph.D. degree in methods and technologies for environmental monitoring from the University of Florence, Florence, Italy, in 1996 and 2001, respectively.

He is presently with the Radar and Radiocommunications Laboratory, Department of Electronic Engineering, University of Florence, and with Consorzio Nazionale Interuniversitario Telecomunicazioni (CNIT), as a Researcher. His main research activity is in the area of remote sensing of rainfall and of the atmosphere through active and passive systems (e.g. spaceborne rain radars and infrared and microwave Earth-satellite links). His current interest is the microwave and infrared spectral analysis of absorption characteristics of the atmosphere components and related attenuation measurements for data processing.

Luca Facheris received the laurea degree (cum laude) in electronic engineering from the University of Florence, Italy, in 1989, and the Ph.D. degree in electronic and information engineering from the University of Padua, Padua, Italy, in 1993.

Since 1993 he has been an Assistant Professor in the Telecommunications area at the Department of Electronic Engineering, University of Florence. His main research activity is in the area of signal and data processing for active remote sensing: radar polarimetry, ground and spaceborne weather radars, and methods for the exploitation of attenuation measurements at microwaves and infrared for remote sensing of the atmosphere.

Simone Tanelli (S'94) received the laurea degree (cum laude) in electronic engineering and the Ph.D. degree in methods and technologies for environmental monitoring from the University of Florence, Florence, Italy, in 1999.

He is currently with the Radar and Radiocommunications Laboratory, Department of Electronic Engineering, University of Florence, and with the Radar Science and Engineering Group, JPL/NASA, Pasadena, CA. His main research activity is in the area of remote sensing of atmosphere. In particular, his research interests include tomographic inversion problems, and spectral analysis of absorption measurements through atmosphere and ground/spaceborne weather radar data processing.

Dino Giuli (M'82–SM'84) received the laurea degree (cum laude) in electronics engineering from the University of Pisa, Pisa, Italy, in 1970.

Since 1973, he has been a Faculty Member, Department of Electronics, University of Florence, Florence, Italy, where he serves now as Full Professor. His research activity has mainly been devoted to experimental and theoretical research in the field of radar systems. He is also involved in research in digital communications and telecommunication networks. His radar research is devoted to optimum processing of dual-polarization radar signals and data and to their integration with data from other spaceborne or ground based sensors.

Prof. Giuli is a member of the Italian Electrical Association (AEI).